DIPLOMARABEIT
Master's Thesis

Towards computer-aided design of biomaterials by example of micro-elasticity of porous ceramic baghdadite ($Ca_3ZrSi_2O_9$)

ausgeführt zum Zwecke der Erlangung des
akademischen Grades eines Diplom-Ingenieurs

unter der Leitung von

Univ.-Prof. Dipl.-Ing. Dr. techn. Christian Hellmich

und

Dipl.-Ing. Maria-Ioana Pastrama

Inst.Nr.: E202
Institut für Mechanik der Werkstoffe und Strukturen

eingereicht an der Technischen Universität Wien
Fakultät für Bauingenieurwesen

von

Hawraa Kariem

Matr.Nr.: 08 26 799
Quadenstrasse 19/10
A – 1220 Wien

Wien, am 11.6.2014

Abstract

Microstructure-elasticity relations for bone tissue engineering scaffolds are key to rationally based biomaterial design.
As a contribution, we here report comprehensive length measuring, weighing, and ultrasonic tests at 0.1 MHz frequency, on porous baghdadite scaffolds.
The resulting porosity-stiffness relations further confirm a formerly detected, micromechanically explained, general relationship for a great variety of different polycrystals (Fritsch et al., 2013), which also allows for estimating the zero-porosity case, i.e. the Young's modulus and Poisson's ratio of pure (dense) baghdadite. These estimates were impressively confirmed by a physically and statistically independent nanoindentation campaign comprising some 1750 indents.
Consequently, we can present a remarkably complete picture of porous baghdadite elasticity across a wide range of porosities, and, thanks to the micromechanical understanding, reaching out beyond classical elasticity, towards poroelastic properties, quantifying the effect of pore pressure on the material system behaviour.

Zusammenfassung

Strukturelle Gerüste (Scaffolds) für die Knochenregeneration aus dem Baghdadit-Keramik($Ca_3ZrSi_2O_9$), mit Porosität zwischen 66% und 94%, wurden auf ihre mechanischen Eigenschaften untersucht.
Die Normalsteifigkeit C_{1111} der Gerüste wurde durch Ultraschalltests mit Longitudinalwellen ermittelt. Anschließend wurden die Ergebnisse der Tests in einem mikromechanischen Model für spröde und poröse Polykristalle (Fritsch et al., 2013) verwendet, um den Elastizitätsmodul E_s und die Querdehnungszahl ν_s der festen Gerüstphase zu erhalten. Die Werte betragen $E_s^{model} = 126$ GPa und $\nu_s^{model} = 0.29$. Zur Überprüfung dieser Werte wurden Nanoindentierungsmessungen durchgeführt, wobei zur Berechnung von E_s^{nano} der Wert der Poissonzahl $\nu_s^{model} = 0.29$ übernommen worden ist. Repräsentierung der Daten von 1750 Indentierungen durch Superposition mehrerer Elastizitätmodul-Normalverteilungen betreffend intakter und geschädigter Kristalle, erlaubt die Indentifikation des E-Moduls der intakten Kristalle als $\bar{E}_s^{nano} = 124$ GPa. Aufgrund der Übereinstimmung von E_s^{model} und $\bar{E}_s^{nano}$, kann auf mögliche Verwendbarkeit des mikromechanischen Modells für die zukünftige computerunterstütze Entwicklung und Herstellung von Baghdadite Scaffolds geschlossen werden.

Acknowledgement

Foremost, I offer my sincere gratitude to my supervisor
Univ. Prof. Dipl.-Ing. Dr. techn. Christian Hellmich, who has supported me throughout the thesis with his knowledge, patience and particularly motivating way.
This research would not have happened without Prof. Peter Pivonka and Prof. Hala Zreiqat, who made such a fruitful cooperation possible.
Dipl.-Ing. Maria-Ioana Pastrama very patiently guided and encouraged me through various steps of the research, which I am very thankful for. I am also thankful to Dipl.-Ing. Krzysztof Wojciech Łuczyński, whose suggestion it was to pursue a thesis at the 'Institute for mechanics of materials and structures'. His knowledge of experimental set-ups was vital. Lab-manager Dr. Andreas Reisinger made sure that everything would run as smoothly as possible. The fact, that he replied to my emails very fast, made my life a lot easier.
Finally, I wish to thank my family for their constant love and support.

Contents

1 Introduction

The research field of biomaterials is fast growing in the last five decades, as the importance of prosthesis and substitute materials for different human tissues is increasing due to an ageing population.
The name of the field was introduced in the 1960's, however, the concept of using foreign materials in the human body is millennia old. The ancient Egyptians used linen for sutures, which are stitches to hold body tissue after an injury, and in Europe fibre from animal intestines were used for the same purpose. Dental implants were also devised in early civilisations, as found in the Mayan culture, where nacre was used to create teeth that even achieved osseointegration, the formation of a direct interface between an implant and bone without fibrous connective tissue.(Ratner et al., 2004)
Different ideas were created and tested throughout history, nonetheless, the success rate was very low due to poor understanding of biocompatibility and sterilization. The probably first in vivo biocompatibility study was conducted by Henry Levert in 1829, who tested different metallic sutures made of gold, silver, lead, and platinum, respectively, on dogs. His findings suggested that platinum was better tolerated than the rest (Levert, 1829). The big breaktrough for metals in medicine came with the creation of stainless steel, as it does not corrode and therefore, allowed surgeons the routine use at reasonable costs (Zierold, 1924).
The turning point for biomaterials came with World War II, the creativity of surgeons to help their patients, and the development of new materials such as high-performance metals, ceramics, and especially polymers. Often in high risk trials, where other options were not available, surgeons tried new materials and procedures, as a life was at stake or the quality of life. While medical results were often not as hoped, these trials lead to an important new order: government quality controls, scientific and engineering input for materials and procedures, and sharing of decisions before attempting new high risk trials (Ratner et al., 2004).
In the 1960's the first generation of modern biomaterials were developed by scientists and engineers from different disciplines, which became the basis for the field of biomaterials. The materials were especially designed for the use inside the human body and their main goal was to mimic the physical properties of the replaced tissue while being bioinert, ideally not causing any toxic response in the body (Hench and Thompson, 2010).

By 1980, three million prosthetic parts, from 50 available prosthesis made from 40 different materials, were implanted worldwide. A characteristic of the first generation materials is their single phase. When implanted in the body, the interface between implant and tissue was an acellular fibrous capsule leading to no or minimal adhesion to the host tissue. This issue lead to the development of the second generation of biomaterials made of composite materials to enable better matched mechanical properties, in order to eliminate or at least minimize stress shielding and bone resorption at the bone-implant interface. Furthermore, the materials were designed to be bioactive, to generate a specific action and reaction in the physiological environment. (Hench and Thompson, 2010)

In orthopaedics various bioactive glasses, ceramics, and glass-ceramics were in clinical trial by the mid 1980's. During the same period, another category of biomaterials became clinically important. The objective of these materials was to be bioresorbable, to break down chemically in a controlled fashion as it is replaced by regenerating tissue. Surgical sutures made from bioresorbable polymers became clinical routine by 1984 (Ratner et al., 2004).

The third generation of biomaterials was introduced with the beginning of tissue engineering in the late 1990's. The focus shifted from replacement to regenerating of tissues on more biological based materials, which can also be cell- and gene-activating (Hench and Thompson, 2010).

One promising field of tissue engineering lies in orthopaedics, as a substitute material for bone is needed due to the high demand. The current gold standard for treating a critical bone defect is autografting, where bone from another part of the patients body, usually the pelvis, is transplanted to the defect site (Calori et al., 2011). The disadvantages of the procedure include the limited supply of available bone, the perioperative and post-operative complications and morbidity associated with the harvesting process (Goulet et al., 1997). The alternative allografting, bone transplant usually harvested from a cadaver, has also major disadvantages, such as the risk of viral disease transmission, immunogenicity and nonunion (Moore et al., 2001). The current clinically approved synthetic bone replacement materials lack in mechanical and biological properties.

As bone is, after blood, the second most transplanted material in the body worldwide (Lewandrowski et al., 2000), there is a high economical incentive to develop substitute materials in bone tissue engineering.

Ideally such materials are porous scaffolds which act as three-dimensional temporary templates to enable colonisation and ingrowth of new cells and

their capillaries. The scaffolds should also be able to carry sufficient load and degrade over time, leaving the bone to remodel naturally (Jones, 2013). The quest to find the most suitable material for bone regeneration has been ongoing since the invention of the first bioactive glass by Larry Hench, which also launched the field of bioactive ceramics (Jones, 2013). The most popular ceramics in clinical application - calcium phosphates, glasses and glass ceramics - either lack in sufficient bioactive properties or in appropriate mechanical properties (Vallet-Regi, 2006), both factors being important for osseointegration. Ceramic scaffolds which are calcium-silicate (Ca-Si) based exhibited excellent bioactivity and degradability (De Aza et al., 2004). The biomaterials and tissue engineering unit of the university of Sydney developed a porous Ca-Si based scaffold, named baghdadite, with the chemical formula $Ca_3ZrSi_2O_9$. The addition of zirconium (Zr) should enhance the mechanical strength and biocompatibility of the scaffolds (Ramaswamy et al., 2008). In various prosthetic devices, the use of Zr showed excellent osseointegration (Kulakov et al., 2005).
The baghdadite scaffolds were tested in rabbits to repair a critical sized bone defect and showed promising results in the histological evaluation (Roohani-Esfahani et al., 2012).
The mechanical properties of these scaffolds are evaluated in the present thesis, especially the scafollds' normal stiffness, the elastic modulus and the Poisson's ratio of a single crystal within the scaffold. Furthermore, a micromechanical model for brittle porous polycrystals (Fritsch et al., 2013) is applied, which shows very good agreement with the experimental results for the mechanical properties of baghdadite scaffolds.

2 Paper entitled 'Micro-poro-elasticity of baghdadite-based bone tissue engineering scaffold: a unifying approach based on ultrasonics, nanoindentation, and homogenization theory' submitted to Acta Biomaterialia

Micro-poro-elasiticity of baghdadite-based bone tissue engineering scaffolds: a unifying approach based on ultrasonics, nanoindentation, and homogenization theory

Hawraa Kariem[a], Maria-Ioana Pastrama[a], Seyed Iman Roohani-Esfahani[b], Peter Pivonka[c], Hala Zreiqat[b], Christian Hellmich[a,*]

[a] *Institute for Mechanics of Materials and Structures, Vienna University of Technology (TU Wien), Karlsplatz 13/202, A-1040 Vienna, Austria*
[b] *Biomaterials and Tissue Engineering Research Unit, School of AMME, The University of Sydney, Sydney 2006, Australia*
[c] *Australian Institute for Musculoskeletal Science, NorthWest Academic Centre, The University of Melbourne, Victoria 3021, Australia*

Abstract

Microstructure-elasticity relations for bone tissue engineering scaffolds are key to rationally based biomaterial design. As a contribution, we here report comprehensive length measuring, weighing, and ultrasonic tests at 0.1 MHz frequency, on porous baghdadite scaffolds. The resulting porosity-stiffness relations further confirm a formerly detected, micromechanically explained, general relationship for a great variety of different polycrystals [J. Appl. Mech 80, 020905-1], which also allows for estimating the zero-porosity case, i.e. the Young's modulus and Poisson's ratio of pure (dense) baghdadite. These estimates were impressively confirmed by a physically and statistically independent nanoindentation campaign comprising some 1750 indents. Consequently, we can present a remarkably complete picture of porous baghdadite elasticity across a wide range of porosities, and, thanks to the micromechanical understanding, reaching out beyond classical elasticity, towards poroelastic properties, quantifying the effect of pore pressure on the material system behaviour.

porous scaffold, mechanical properties, nanoindentation, ultrasound, micromechanical model

1. Introduction

With an estimated 2.2 million yearly bone graft procedures for the treatment of critical size defects, bone is the second-most implanted material after blood [1]. Despite considerable progress over the years, the current gold standard, autografting [2], where bone from the patient is transplanted from one place to another, is limited by the amount of bone available, and may imply pre- and post-operative complications and morbidity, as well as the risk of infection [3]. The current clinical alternative, allografting, where cadaveric or synthetic bone is implanted, carries the risk of viral disease transmission, immunogenicity, and nonunion [4]. This has motivated, for more than two decades, research in the field of bone tissue engineering [5–8], aiming at repairing damaged bone and restoring its functions with the help of biocompatible materials cultivated with cells and corresponding growth factors. Therefore,

*Corresponding author. Tel.: +43 1 58801 20220; Fax: +43 1 58801 20299
Email address: christian.hellmich@tuwien.ac.at (Christian Hellmich)

the scaffolds have to be designed in a way providing sufficient pore space for the biological cells to resorb the scaffold material and to generate new tissue, while not overly compromising the overall mechanical properties of the implant, i.e. its stiffness and strength. This design process, involving also the biological properties of the implant material, turns out as very complex, and implies many design parameters whose interplay is extremely challenging to decipher in a classical 'trial-and-error' procedure, requiring a sheer innumerable multitude of *in vitro* and *in vivo* experiments. This challenging situation has given rise to the wish for rational, computer-aided design of biomaterials, regarding not only biological and cell transport aspects, but also mechanics. The present paper will concentrate on the latter aspect, thereby not being restricted to the measurement of some mechanical properties, but to a micromechanics theory-based understanding of an entire class of ceramic biomaterials, supported by a new set of experimental data making the aforementioned understanding feasible. More precisely, we will develop the micromechanics of porous baghdadite scaffolds - these materials showed *in vivo* osteoconductivity in critically sized defects induced into rabbit radius bones, which exceeds that of other scaffold types [9]. These developments will be described in the remainder of the present paper, which is organized as follows: porosity and ultrasonic test protocols together with their theoretical foundations will be dealt with in Section 2.1. For a deeper understanding of the resulting porosity-elasticity relations, Section 2.2 will cover a micromechanics formulation valid for a multitude of porous polycrystals, as developed in recent years [10–12], and its application to the newly collected experimental data. This will give access to the elastic properties of pure (dense) baghdadite. The methods section is then completed by a nanoindentation campaign allowing for an independent check of elasticity of pure baghdadite, as described in Section 2.3. The results of our comprehensive and consistent experimental-theoretical-computational multiscale mechanics approach to baghdadite scaffolds for bone tissue engineering are presented in Section 3, and further discussed in Section 4, in particular with respect to important theoretical and experimental features which allow for this consistent, unified view on the investigated bone biomaterial class.

2. Materials and methods

2.1. Weighing and ultrasonic tests, for porosity and elasticity determination

Combining the sol-gel method for powder production with the polymer sponge replication method for the final scaffold processing [9], cylindrically shaped porous baghdadite samples of nominally 12 mm height and 6 mm diameter were made, and categorized with decreasing nominal porosities, into sample sets A to D. Their precise dimensions of height and diameter were measured by means of a digital sliding calliper, and these dimensions were used to compute the cylindrical volume V of each of the samples. Then, their mass m was weighed, giving access to the samples' mass density through

$$\rho = m/V \tag{1}$$

Additional consideration of the (real) mass density of pure (dense) baghdadite, $\rho_{solid} = 3.48$ g/cm^3 [13], allows for computation of the scaffold porosity as

$$\phi^{exp} = (1 - \rho/\rho_{solid}) \tag{2}$$

Thereafter, ultrasonic tests were performed in the pulse transmission mode, by means of a device consisting of a pulser-receiver (5077PR, Olympus NDT), an oscilloscope (Waverunner 62Xi, Lecroy), and ultrasonic transducers. Following the protocol of [14, 15] the pulser unit was set to emit an electrical square pulse up to 400 V. The piezoelectric elements inside the ultrasonic transducers transformed the electrical signals of a frequency f into corresponding mechanical signals, when operating in the sending mode, or they transformed mechanical signals back to electrical ones, when functioning as a receiver. Honey was used as a coupling medium. The time of flight t of the ultrasonic wave through the sample was accessed by the oscilloscope and the travel distance through the specimen was equivalent to the scaffold's height h. These quantities provide direct access to the wave velocity v through

$$v = h/t \tag{3}$$

According to the theory of plane waves in a 3D solid [16], the wave velocity gives access to the stiffness of the tested sample. The current study is restricted to longitudinal waves where the directions of 'particle' displacement and of the wave propagation are parallel - in this case, the wave velocity gives access to the normal component C^{exp}_{1111} of the stiffness tensor, through

$$C^{exp}_{1111} = \rho v^2 \tag{4}$$

What still needs to be specified is the size at which the aforementioned 'particle' is defined. In continuum (micro)mechanics [17], such a 'particle' is called material volume or representative volume element (RVE), with a characteristic length l_{RVE} being considerably larger than the inhomogeneities d within the RVE, and the RVE being subjected to homogeneous stress and strain states. Consequently, the characteristic length l_{RVE} needs to be much smaller than the scale of the characteristic loading of the medium, here the wavelength λ, which follows from wave velocity v and frequency f as

$$\lambda = v/f \tag{5}$$

The aforementioned separation of length scales reads mathematically as

$$d \ll l_{RVE} \ll \lambda \tag{6}$$

Accordingly, ultrasonic waves with wavelength λ detect the stiffness of a material with characteristic length l_{RVE}. More precisely, the '$\ll$' signs in Eq.(6) need to refer to a ratio of $d/\lambda \leq 0.3$, in order to access the normal stiffness component C_{1111} of the tested material with inhomogeneity size d, as was experimentally quantified in [15]. As for the aforementioned baghdadite samples, the inhomogeneity size relates to the pore diameters, amounting to about 500 μm, as accessed by scanning electron microscopy [9]. In order to check different options for determination

of C_{1111}^{exp} according to Eq.(4), while considering scale separation conditions (6), the samples were sonified with a frequency of 0.1 MHz.

2.2. Polycrystal micromechanics - elastic properties of pure (dense) baghdadite

The porosity - stiffness relations determined experimentally according to Section 2.1 were then evaluated within the framework of continuum micromechanics (or random homogenization [17, 18]) of porous polycrystals, developed in recent years for RVEs consisting of one porous phase and infinitely many, disc- or needle-shaped crystal phases oriented in different space directions [10–12]. More specifically, a large number of porosity and stiffness data from different isotropic materials, such as hydroxyapatite [19–22], bioactive glass-ceramics (CEL2) [23], gypsum [24–28], various piezoelectric ceramics [29], alumina [30–32], zirconia [32], as well as silica and nitride carbides [33–35], could be integrated into only *two* crystal shape- (i.e. needle- or disc-) specific scaling relations for the polycrystals' (homogenized) Young's modulus. Both relations can then be approximated by a power function reading as [12]

$$E^{hom}/E_s \simeq \mathcal{B}_E(1-\phi)^{C_E} \tag{7}$$

with E^{hom} as the Young's modulus of the overall porous polycrystal, E_s as the Young's modulus of the single crystal, and $\mathcal{B}_E$ and C_E as crystal shape-specific coefficients. Earlier obtained images [9] suggest the baghdadite crystals to be disc-shaped, with corresponding coefficients $\mathcal{B}_E = 0.9867$ and $C_E = 2.053$ [12], and an overall Poisson's ratio which only depends on that of the single crystals, ν_s, and on the porosity ϕ, following a polynomial approximation

$$\nu^{hom} = \bar{\mathcal{A}}_\nu(1-\phi)^4 + \bar{\mathcal{B}}_\nu(1-\phi)^3 + \bar{\mathcal{C}}_\nu(1-\phi)^2 + \bar{\mathcal{D}}_\nu(1-\phi) + \bar{\mathcal{E}}_\nu \tag{8}$$

with the coefficients fulfilling a linear relation of the format

$$q = a^*\nu_s + b^*, \text{ with } q = \bar{\mathcal{A}}_\nu, \bar{\mathcal{B}}_\nu, \bar{\mathcal{C}}_\nu, \bar{\mathcal{D}}_\nu, \bar{\mathcal{E}}_\nu \tag{9}$$

see Table 1 for values of a^* and b^*. Young's modulus and Poisson's ratio give access to the stiffness component C_{1111}, whereby E_s and ν_s follow the scaling relations in Eq.(7) and Eq.(8), so that

$$C_{1111}^{hom} = \frac{E^{hom}(E_s,\phi)\times[1-\nu^{hom}(\nu_s,\phi)]}{[1+\nu^{hom}(\nu_s,\phi)]\times[1-2\nu^{hom}(\nu_s,\phi)]} \tag{10}$$

Minimizing the mean absolute error between micromechanics-based stiffness expression (10) evaluated for experimentally determined porosities ϕ_i^{exp}, and corresponding experimentally determined stiffness values $C_{1111}^{exp,i}$,

$$\sum_j \left\| C_{1111}^{hom}(\phi_i^{exp}, E_s\nu_s) - C_{1111}^{exp,i} \right\| \rightarrow \min. \tag{11}$$

provides an estimate for the elastic properties of pure (dense) baghdadite.

Table 1: Coefficients a^* and b^* defining linear relation (9) between Poisson's ratio of single crystals, ν_s, and polynomial coefficients $\bar{\mathcal{A}}_\nu, \bar{\mathcal{B}}_\nu, \bar{\mathcal{C}}_\nu, \bar{\mathcal{D}}_\nu, \bar{\mathcal{E}}_\nu$ in porosity-Poisson's ratio relation (8).

q	a^*	b^*
$\bar{\mathcal{A}}_\nu$	-1.0521	0.2197
$\bar{\mathcal{B}}_\nu$	2.2684	-0.4645
$\bar{\mathcal{C}}_\nu$	-0.8121	0.1662
$\bar{\mathcal{D}}_\nu$	0.3602	-0.0718
$\bar{\mathcal{E}}_\nu$	0.2394	0.1496

2.3. Nanoindentation

In order to provide a check for the estimated properties of pure baghdadite, according to Section 2.2, from experimentally determined porosity-stiffness relations and polycrystal micromechanics, a nanoindentation campaign comprising some 1750 indents was performed. For this, one sample was chosen from each of the sample sets A to D. Following the protocol in [36], these samples were then embedded in resin (Epofix, Struers, Denmark), and held in a vacuum chamber for 10 minutes to eliminate air bubbles, before being dried for 48 hours. Afterwards, the embedded samples were cut into 2 mm thick sections by means of a water-cooled low speed saw (IsoMet, Buehler), and glued onto object slides. This enabled subsequent polishing, first through a polishing machine (PM5, Logitech, Scotland) with increasingly fine sandpaper, and eventually, with a napped cloth impregnated with 3 μm small diamond grains, see Table 2 for details of the polishing protocol. Due to their high porosity, samples from set A displayed very limited solid surfaces for testing. Therefore, two scaffolds from this set were prepared for nanoindentation, in order to allow for a sufficient number of measurements. The nanoindentation tests (Nano Hardness Tester, CSM, Switzerland) were performed with a Berkovich tip in the load-controlled mode. The loading- unloading rate was set at 30 mN/min, the holding time was 10 seconds, and four different maximum loads were used: 10, 15, 20, 30 mN. The specific measurement details are given in Table 3. Although two scaffolds from set A were prepared for indentation, there was still not enough surface to perform as many measurements as on samples from the other sets. Thus, no tests with a maximum load of 30 mN were performed. The 1750 measurements were evaluated according to the method of Oliver and Pharr [37], which states that the elastic unloading stiffness S is defined as the slope of the unloading curve during the initial stages of unloading. The relationship between the stiffness S, the contact area A, and the reduced elastic modulus E_r is given by

$$S = \frac{2}{\sqrt{\pi}} E_r \sqrt{A} \tag{12}$$

The reduced modulus E_r takes into account that elastic displacements occur in both the substrate - here a dense (pure) baghdadite crystal with elastic modulus E_s and Poisson's ratio ν_s - and in the Berkovich indenter with elastic modulus E_i and Poisson's ratio ν_i,

$$1/E_r = (1 - \nu_i^2)/E_i + (1 - \nu_s^2)/E_s \tag{13}$$

The elastic properties of the diamond indenter are known and considered in the indentation software: $E_i = 1141$ GPa and $\nu_s = 0.07$ [37, 38].

Table 2: Polishing protocol

Step	Sandpaper	Time [min]	Arm	Plate Speed [rpm]
1	2400 Grit	3	Sweeping	18
2	4000 Grit	5	Sweeping	25
3	3µm	4	Sweeping	25

Table 3: Number of nanoindentation measurements per sample and per load

Sample	ϕ [%]	Maximum Load [mN]	Measurements
A2	94	10	22
A8		10	56
		15	39
		20	33
B8	85	10	50
		15	50
		20	50
		30	50
C3	81	10	50
		15	50
		20	50
		30	50
D1	66	10	300
		15	300
		20	300
		30	300

Hence, combination of (12) and (13) allows for expressing the Young's modulus of pure baghdadite as a function of the unloading stiffness S, and of E_i, ν_i, and ν_s,

$$E_s = \left(\frac{S\sqrt{\pi}}{2\sqrt{A}} - \frac{E_i}{1-\nu_i^2}\right)\left(1-\nu_s^2\right) \tag{14}$$

where the value for ν_s is adopted from the results corresponding to Section 2.2. Analysis of 1750 values for E_s according to (14) follows the concept of the statistical or grid nanoindentation method [39–41]. This method is based on the statistical analysis of a large number of indentation-derived values of a mechanical property such as Young's modulus E_s. In more detail, the measured data are first used to generate the experimental Cumulative Distribution Function (CDF): The number of indentations N and the sorted values of elastic modulus E_s deliver the N points D_{E_s} of the experimental CDF,

$$D_{E_s}(E_{s,i}) = \frac{i}{N} - \frac{1}{2N} \tag{15}$$

with $i \in [0; N]$, $N = 1750$ the number of indentations. The key premise of the statistical indentation method is then

to approximate the CDF by superposition of a number of CDFs related to the individual material phases making up the substrate which is subjected to grid nanoindentation. While earlier applications of the method discriminated the material phases according to their different chemical natures, we here consider different mechanical properties arising from changes induced in the substrate material through the indentation testing itself: The loads to which the substrate is subjected to are likely to sometimes induce cracking (or damage) of the material, a phenomenon which is known to occur also in the context of nanoindentation of bone with a protocol similar to ours, see e.g. [42]. This implies that at least two material phases are expected in the tested substrate: (i) intact baghdadite, and (ii) one damaged phase (or several different damaged phases related to different crack sizes or densities, representing somehow the 'fractal' nature of cracking). After representing the mechanical effect of all the phases by means of Gaussian distributions

$$D(E_{s,i};\mu_j,s_j) = \frac{1}{s_j\sqrt{2\pi}}\int_{-\infty}^{E_{s,i}} \exp\left(\frac{-(u-\mu_j)^2}{2s_j^2}\right)du \tag{16}$$

with the mean value μ_j and standard deviation s_j of each phase, we fit the experimental CDF by n model CDFs with weighting factors (or volume fractions) f_i, $\sum_{i=1}^{n} f_i = 1$, through minimization of the following error

$$Error = \sum_{i=1}^{N}\left(\sum_{j=1}^{n} f_j D(E_{s,i};\mu_j,s_j) - D_{E_s}(E_{s,i})\right)^2 \rightarrow \min. \tag{17}$$

The minimization procedure itself is performed by an evolutionary strategy, as described in the Appendix. We realize this optimization procedure for different numbers of phases, and we check whether the number of chosen phases, $n \geq 2$, has an effect on the mean value of the rightmost CDF (relating to the Young's modulus of pure baghdadite), and whether the latter agrees with that obtained according to Section 2.2. Thereby, the goodness of fit is measured through the coefficient of determination R^2, and the relative error e_{rel} in %, which is defined as

$$e_{rel} = 100 \times \sum_{i=1}^{N}\left[1 - \frac{D(E_{s,i};\mu_j,s_j)}{D_{E_s}(E_{s,i})}\right] \tag{18}$$

3. Results

3.1. Porosity and elasticity determination

The porosity of the investigated porous baghdadite samples ranged between 66% and 94%, see Table 4 for sample set-specific details. The corresponding normal stiffness components C_{1111}^{exp} ranged from 0.98 to 15.16 GPa, see Table 5. These stiffness components monotonously decrease with increasing porosity, see Table 6 and Figure 1. The corresponding wavelengths according to Eq.(5) with $f = 0.1$ MHz and v as reported in Table 5, ranged from 1.40 to 3.88 cm, hence, they fulfil the separation of scales requirement given in Eq.(6) for $d = 500$ μm, and correspondingly, the derived stiffness values ranging from 0.43 to 17.27 GPa indeed refer to the overall porous baghdadite scaffold material.

Table 4: Weight, dimensions, mass density, and porosity of tested baghdadite samples

Sample	Weight [g]	Height [cm]	Diameter [cm]	Volume [cm^3]	ρ [g/cm^3]	ϕ [%]
A1	0.108	1.274	0.656	0.431	0.251	93
A2	0.077	1.237	0.598	0.347	0.222	94
A3	0.127	1.203	0.625	0.369	0.344	90
A4	0.108	1.263	0.611	0.370	0.292	92
A5	0.111	1.291	0.627	0.399	0.278	92
A6	0.103	1.166	0.670	0.411	0.251	93
A7	0.132	1.273	0.616	0.379	0.348	90
A8	0.076	1.190	0.607	0.344	0.221	94
B1	0.142	1.302	0.603	0.372	0.382	89
B2	0.154	1.272	0.652	0.425	0.363	90
B3	0.151	1.263	0.638	0.404	0.374	89
B4	0.142	1.349	0.620	0.407	0.349	90
B5	0.195	1.368	0.617	0.409	0.477	86
B6	0.134	1.201	0.630	0.374	0.358	90
B7	0.146	1.271	0.630	0.396	0.368	89
B8	0.211	1.343	0.628	0.416	0.507	85
B9	0.133	1.247	0.637	0.397	0.335	90
B10	0.197	1.349	0.649	0.446	0.441	87
B11	0.126	1.212	0.633	0.381	0.330	91
C1	0.240	1.268	0.628	0.393	0.611	82
C2	0.244	1.326	0.608	0.385	0.634	82
C3	0.274	1.211	0.656	0.409	0.669	81
C4	0.236	1.319	0.642	0.427	0.553	84
C5	0.274	1.265	0.681	0.461	0.595	83
C6	0.282	1.286	0.618	0.386	0.731	79
C7	0.215	1.164	0.618	0.349	0.616	82
C8	0.267	1.300	0.664	0.450	0.593	83
C9	0.219	1.299	0.637	0.414	0.529	85
C10	0.221	1.280	0.645	0.418	0.528	85
D1	0.520	1.348	0.657	0.457	1.138	67
D2	0.484	1.252	0.656	0.423	1.144	67
D3	0.456	1.246	0.641	0.402	1.134	67
D4	0.508	1.330	0.662	0.458	1.110	68
D5	0.453	1.245	0.649	0.412	1.100	68
D6	0.430	1.174	0.675	0.420	1.024	71
D7	0.419	1.208	0.675	0.432	0.969	72
D8	0.504	1.237	0.659	0.422	1.195	66

Table 5: Mass density ρ, time of flight t_f, height h, wave velocity v, and normal stiffness component C_{1111}^{exp} of baghdadite samples obtained through ultrasonic testing

Sample	ρ [kg/m^3]	t_f [s]	h [m]	v [m/s]	C_{1111}^{exp} [GPa]
A1	2.51×10^{2}	5.90×10^{-6}	1.27×10^{-2}	2.16×10^{3}	1.17
A2	2.22×10^{2}	8.84×10^{-6}	1.24×10^{-2}	1.40×10^{3}	0.43
A3	3.44×10^{2}	6.96×10^{-6}	1.20×10^{-2}	1.73×10^{3}	1.03
A4	2.92×10^{2}	6.73×10^{-6}	1.26×10^{-2}	1.88×10^{3}	1.03
A5	2.78×10^{2}	6.37×10^{-6}	1.29×10^{-2}	2.03×10^{3}	1.15
A6	2.51×10^{2}	6.36×10^{-6}	1.17×10^{-2}	1.83×10^{3}	0.84
A7	3.48×10^{2}	5.93×10^{-6}	1.27×10^{-2}	2.15×10^{3}	1.61
A8	2.21×10^{2}	7.45×10^{-6}	1.19×10^{-2}	1.60×10^{3}	0.56
B1	3.82×10^{2}	6.47×10^{-6}	1.30×10^{-2}	2.01×10^{3}	1.55
B2	3.63×10^{2}	5.62×10^{-6}	1.27×10^{-2}	2.26×10^{3}	1.86
B3	3.74×10^{2}	5.77×10^{-6}	1.26×10^{-2}	2.19×10^{3}	1.79
B4	3.49×10^{2}	5.36×10^{-6}	1.35×10^{-2}	2.52×10^{3}	2.21
B5	4.77×10^{2}	5.61×10^{-6}	1.37×10^{-2}	2.44×10^{3}	2.84
B6	3.58×10^{2}	5.75×10^{-6}	1.20×10^{-2}	2.09×10^{3}	1.56
B7	3.68×10^{2}	5.52×10^{-6}	1.27×10^{-2}	2.30×10^{3}	1.96
B8	5.07×10^{2}	5.85×10^{-6}	1.34×10^{-2}	2.30×10^{3}	2.67
B9	3.35×10^{2}	5.45×10^{-6}	1.25×10^{-2}	2.29×10^{3}	1.75
B10	4.41×10^{2}	5.54×10^{-6}	1.35×10^{-2}	2.43×10^{3}	2.62
B11	3.30×10^{2}	6.59×10^{-6}	1.21×10^{-2}	1.84x10^3	1.12
C1	6.11×10^{2}	4.75×10^{-6}	1.27×10^{-2}	2.67×10^{3}	4.36
C2	6.34×10^{2}	4.84×10^{-6}	1.33×10^{-2}	2.74×10^{3}	4.76
C3	6.69×10^{2}	4.04×10^{-6}	1.21×10^{-2}	3.00×10^{3}	6.02
C4	5.53×10^{2}	5.64×10^{-6}	1.32×10^{-2}	2.34×10^{3}	3.03
C5	5.95×10^{2}	4.96×10^{-6}	1.27×10^{-2}	2.55×10^{3}	3.87
C6	7.31×10^{2}	4.87×10^{-6}	1.29×10^{-2}	2.64×10^{3}	5.09
C7	6.16×10^{2}	5.12×10^{-6}	1.16×10^{-2}	2.27×10^{3}	3.18
C8	5.93×10^{2}	5.60×10^{-6}	1.30×10^{-2}	2.32×10^{3}	3.20
C9	5.29×10^{2}	5.63×10^{-6}	1.30×10^{-2}	2.31×10^{3}	2.82
C10	5.28×10^{2}	5.06×10^{-6}	1.28×10^{-2}	2.53×10^{3}	3.39
D1	1.14×10^{3}	3.70×10^{-6}	1.35×10^{-2}	3.65×10^{3}	15.13
D2	1.14×10^{3}	3.29×10^{-6}	1.25×10^{-2}	3.81×10^{3}	16.57
D3	1.13×10^{3}	3.37×10^{-6}	1.25×10^{-2}	3.70×10^{3}	15.53
D4	1.11×10^{3}	3.54×10^{-6}	1.33×10^{-2}	3.76×10^{3}	15.65
D5	1.10×10^{3}	3.26×10^{-6}	1.25×10^{-2}	3.82×10^{3}	16.04
D6	1.02×10^{3}	3.67×10^{-6}	1.17×10^{-2}	3.20×10^{3}	10.48
D7	9.69×10^{2}	3.11×10^{-6}	1.21×10^{-2}	3.88×10^{3}	14.61
D8	1.19×10^{3}	3.25×10^{-6}	1.24×10^{-2}	3.80×10^{3}	17.27

Table 6: Mean value and standard deviation of normal stiffness C_{1111}^{exp} of baghdadite scaffolds obtained through ultrasonic testing

Sample	$\bar{\phi}$ [%]	$\bar{C}_{1111}^{exp}$ [GPa]
A	92±1	0.98±0.34
B	89±2	1.99±0.51
C	83±2	3.97±1.00
D	68±2	15.16±1.93

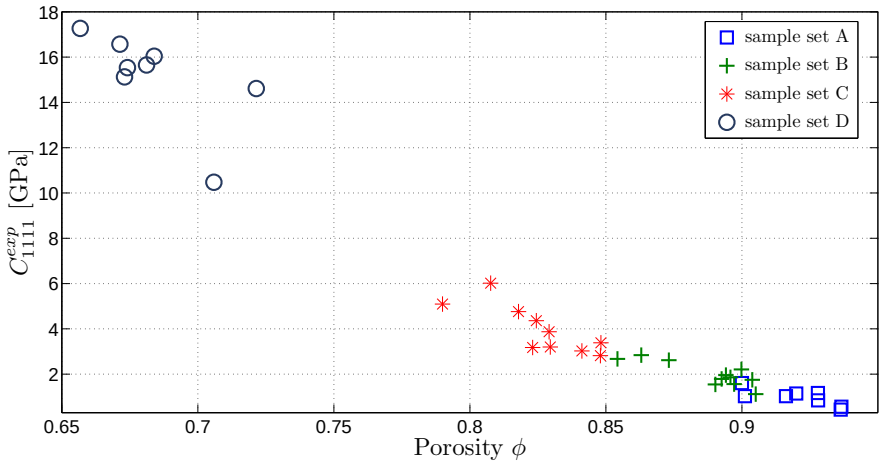

Figure 1: Normal stiffness of baghdadite scaffolds C_{1111}^{exp} determined by ultrasonic testing for the four different sample sets A, B, C, D. The stiffness C_{1111}^{exp} increases with decreasing porosity ϕ.

3.2. Elastic properties of pure (dense) baghdadite

The aforementioned stiffness-porosity relation can be very well predicted by the micromechanics model (7) - (10): Optimization procedure (11) resulted in a fit characterized by a relative error of $e_{rel}^{C_{1111}} = -4.12\%$ and a coefficient of determination of $R^2 = 0.98$, see Figure 2. The corresponding elastic properties of pure (dense) baghdadite amount to $E_s^{US} = 126$ GPa and $\nu_s^{US} = 0.29$. Their reliability is expressed through a comparison with the 1750 results from the nanoindentation campaign, depicted in the form of a (normalized) histogram in Figure 3. They are virtually optimally represented by a superposition of five Gaussian distribution functions, relating to a relative error amounting to only 0.006%, and a correlation coefficient of $R^2 = 99.9\%$, see Table 7. Accordingly, the corresponding black line in Figure 3 very accurately follows the trend given by the histogram columns, and an even more impressive, almost perfect match between experimental and theoretical CDFs is observed in Figure 4. The rightmost Gaussian distribution relates to the non-damaged baghdadite, i.e. to the state of the solid scaffold material also expected in ultrasonically tested scaffolds. Indeed, its mean value of $\bar{E}_s^{NI} = 124$ GPa agrees almost perfectly with $E_s^{US} = 126$ GPa obtained from the micromechanical evaluation of the ultrasonic tests. By example, a typical load-displacement curve corresponding to a nano-indented non-damaged baghdadite crystal is depicted in Figure 5.

Table 7: Superposition results of n Gaussian distributions fitted to the experimental CDF which was obtained from 1750 nanoindentation measurements of baghdadite substrate; values of Young's Modulus $\bar{E}_s^{NI}$, weighting factor f_i, and the goodness of fit measurements refer to the rightmost distribution

n Distributions	$\bar{E}_s^{NI}$ [GPa]	f_i [%]	R^2	e_{rel}^{NI} [%]
2	124.2	37.52	0.8821	-27.810%
3	127.4	26.99	0.9547	8.780%
4	122.5	27.97	0.9917	2.130%
5	123.7	26.38	0.9993	0.006%
6	127.2	32.76	0.9941	-1.530%

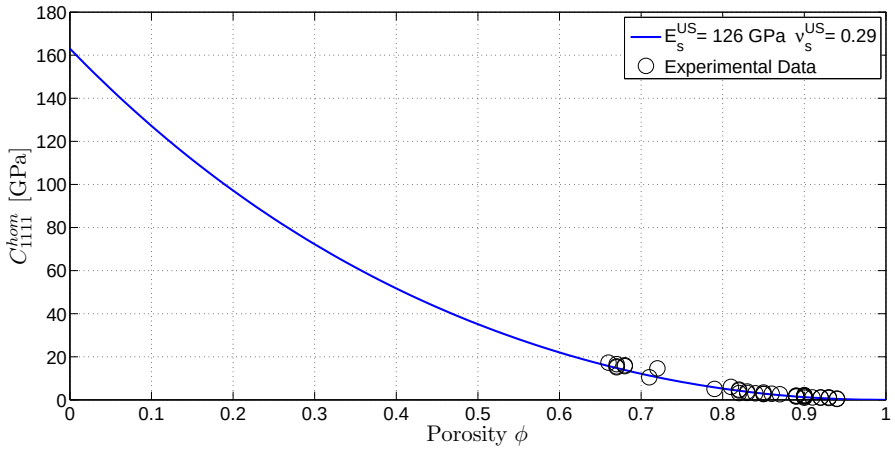

Figure 2: Porosity-stiffness relation for porous baghdadite scaffolds, from optimizing micromechanics model response [12] for length measuring, weighing, and ultrasonic test results of Table 4 and 5; this provides elastic properties of pure (dense) baghdadite, E_s^{US}, and ν_s^{US}

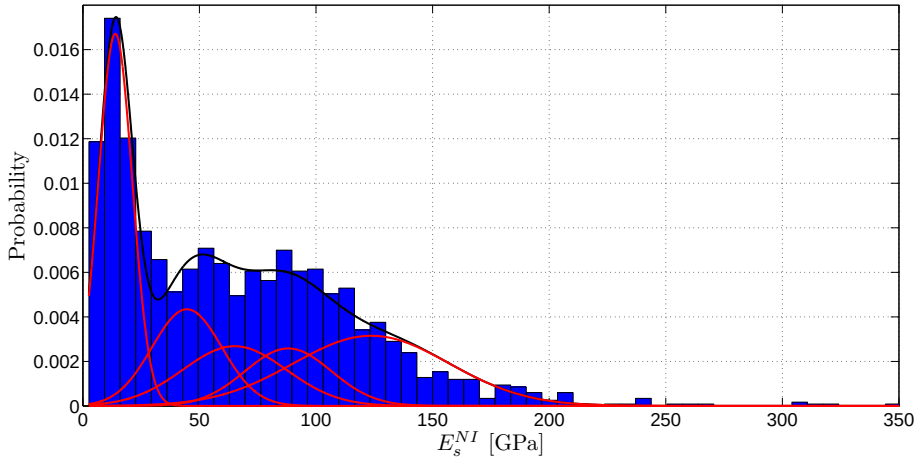

Figure 3: Histogram of elastic moduli obtained from nanoindentation measurements and representation through contribution of five material phases, the stiffest of which is pure (non-damaged) baghdadite

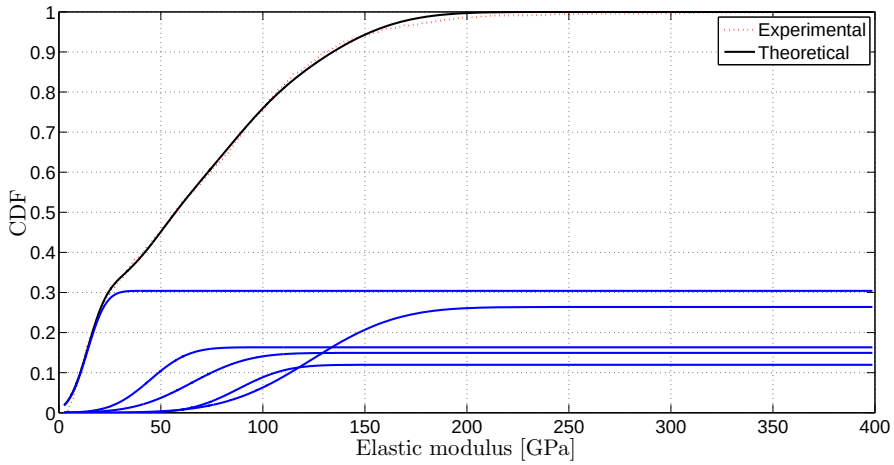

Figure 4: Experimental CDF obtained by nanoindentation, and the five theoretical Gaussian CDFs obtained by deconvolution according to the statistical nanoindentation method of [39–41]

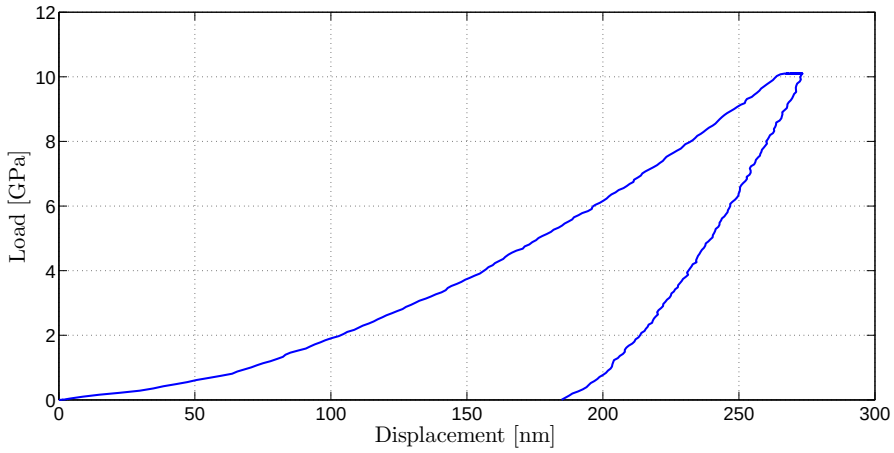

Figure 5: Typical load-displacement curve of a non-damaged single crystal of the baghdadite scaffolds, with an obtained elastic modulus of E_s^{NI} = 124.7 GPa at 10mN maximal load

4. Discussion

While the current state-of-the-art in mechanical characterization of biomaterials is defined by the measurement of a few selected mechanical properties in mostly standardized mechanical testing devices, we here go a step forward, towards a unified understanding of the mechanical functioning of an entire material class - porous scaffolds for bone tissue engineering made of baghdadite - which itself turned out to be part of yet a larger material class encompassing numerous different porous (glass-) ceramic systems. In more detail, continuum micromechanics was used as a versatile theoretical and computational frame, allowing for deriving structure-property relations in the form of elasticity functions with the porosity as an argument, these functions being experimentally validated by various physically and statistically independent experiments, namely weighing, ultrasound, and nanoindentation tests. It is not the first time that such tests have been performed on biomaterials (although mechanical testing of baghdadite appears as a quite rare occurrence in literature), but the consistent emergence of just one overall picture of scaffold behaviour arising from all the different tests is indeed considered as something original and remarkable. The aforementioned consistency critically depends on careful evaluation of experimental data, taking into account important theoretical concepts underlying the used experimental devices. In this context, the following features of our evaluation method are particularly noteworthy:

- While the sample dimensions qualify them as fairly 'thick' beams, and classical mechanical tests when driven in unloading mode [43] would certainly deliver a Young's modulus E of the tested material, it is important to remember that ultrasonic tests in most of the cases deliver the normal stiffness component C_{1111}, rather than a Young's modulus. Actually, the tested beams need to be extremely slender to allow for an extensional wave to propagate along a beam-type sample, and systematic studies of [15] have shown that as long as

$$A \log\left(\frac{d}{h}\right) + B \log\left(\frac{h}{\lambda}\right) \leq 1 \tag{19}$$

  with $A = -1.426$ and $B = -0.530$, bulk wave propagation related to a 3D solid with normal stiffness C_{1111} occurs. For all the tests reported in the present paper, the left-hand side of (19) ranges from 0.45 to 0.67, therefore the samples behaved as 3D solids.

- Given the fact that ultrasonic tests deliver C_{1111} rather than E, they cannot be simply compared to some more or less empirical relation concerning Young's modulus, but need to be related to some more complete description of the material behaviour - in the present case, this description was provided by continuum micromechanics, which delivered the full elasticity tensor, which in the case of isotropic materials, as encountered here, can be expressed in terms of Young's modulus *and* Poisson's ratio, the latter two defining, therefore, also the stiffness component C_{1111}.

- Another critical issue with ultrasonic tests is the choice of a suitable frequency - once the corresponding wavelength does not fulfil the separation-of-scales criteria (6) anymore (a case *not* encountered here), the velocity of

the ultrasonic wave is not related to the components of the elasticity tensor, i.e. ultrasound cannot be used for elasticity characterization of biomaterials anymore.

- The probably most remarkable feature of the present evaluation as compared to earlier scientific endeavours is the use and application-specific adaptation of the statistical nanoindentation method. Rather than averaging over the results of a few tests, or checking nanoindentation size effect laws [44] (see Figure 6 for a corresponding evaluation of our nanoindentation results), which could not have provided access to the elasticity of pure baghdadite, we identified the indented substrate as being composed of one intact crystal phase and several mechanically damaged phases. This provided elastic properties being absolutely in line with those obtained from micromechanics-based ultrasound evaluation.

The herein introduced and validated micromechanics model of porous baghdadite allows for prediction well beyond elasticity: In continuum micromechanics, an RVE cannot only be subjected to stress and strain states at its outer boundary, but also to a pore pressure acting within the pore space. Hence, once the upscaling from the single crystal elasticity to the overall porous polycrystal is achieved, also the key poroelastic properties are known [12, 18]. They are (i) the Biot coefficient quantifiying the stress arising at the undeformed boundary of the RVE, from internal pore pressure (see Figure 7a), and (ii) the Biot modulus quantifying the porosity change within an RVE whose boundary is undeformed, again arising from pore pressure (see Figure 7b). Equipped with this information, the elastic deformation arising from any external or internal stress states acting, under physiological conditions, on implanted porous baghdadite scaffolds can be determined. This is considered as a firm basis for computer-aided design or safety assessment of such scaffolds. In order to complete the latter, our current research activities are directed towards strength upscaling, based on already achieved success for biomaterials made of hydroxyapatite [10–12], glass-ceramics [23], or titanium [45].

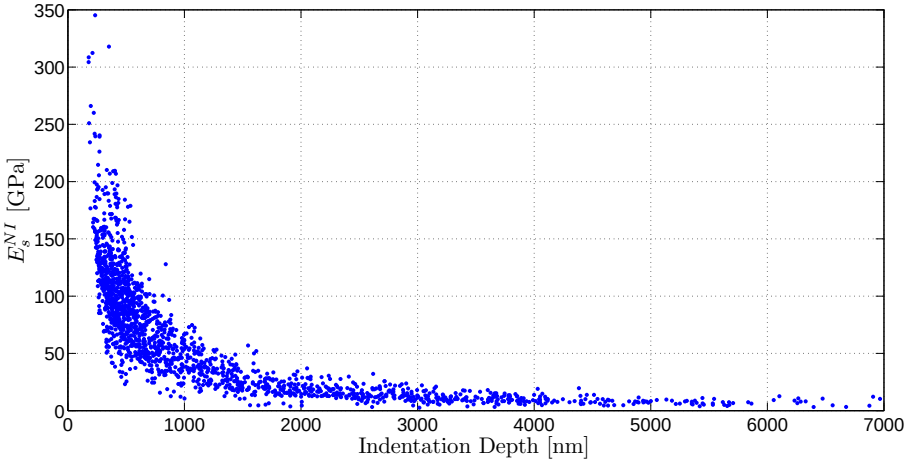

Figure 6: Nanoindentation size effect in baghdadite scaffolds: Young's modulus E_s^{NI} as a function of indentation depth

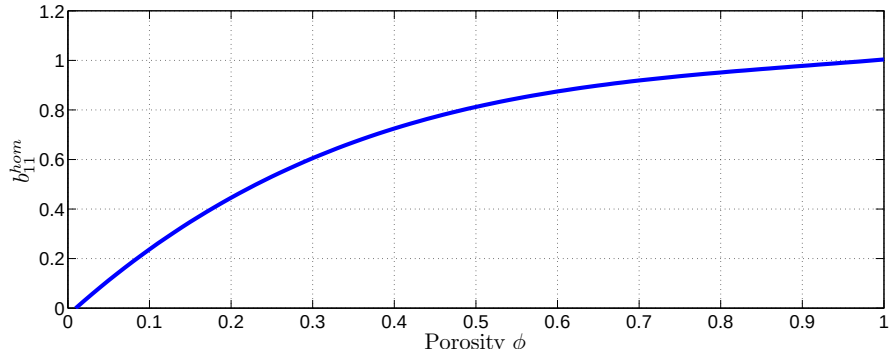

(a)

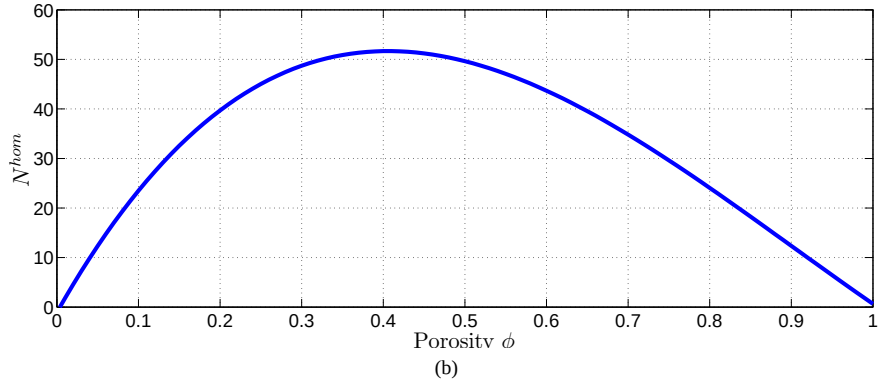

(b)

Figure 7: Poro-elasticity of porous baghdadite scaffolds: (a) Biot coefficient as function of porosity; (b) Biot modulus as function of porosity

Appendix

Evolutionary strategy

The evolutionary strategy assumes the starting parameters, the distribution's mean value μ_0^g, variance σ_0^g and weighting factor f_i^g, as 'parents' X_P^g:

$$X_P^g = \left\{\mu_0^g, \sigma_0^g, f_0^g\right\} \tag{20}$$

The strategy involves three subsequent steps:

(I) **Mutation**. In the first step, the starting parameters are mutated by adding a normally distributed random number to the parents,

$$X_m^g = X_P^g + Z^g\sigma, \tag{21}$$

where Z_g is generated from a normal distribution $\nu(0, \sigma^m(\alpha))$, with mean 0 and standard deviation equal to the scattering parameter $\sigma(\alpha)$, α being the step size, $\alpha = 0.85$ [46].

This results into a new, mutated parent, with its mutated parameters:

$$X_m^g = \left\{\mu_m^g, \sigma_m^g, f_m^g\right\} \tag{22}$$

(II) **Recombination**. In the next step, through recombination of the starting and the mutated parameters, one obtains a series of possible combinations of parameters $\left\{\mu_i^g, \sigma_j^g, f_k^g\right\}$. As the mean value and standard deviation should stem from the same group, $i = j$, only four combinations remain possible, out of which three are the newly generated 'offsprings',

$$\begin{aligned} X_{O_1}^g &= \left\{\mu_0^g, \sigma_0^g, f_m^g\right\} \\ X_{O_2}^g &= \left\{\mu_m^g, \sigma_m^g, f_0^g\right\} \\ X_{O_3}^g &= \left\{\mu_m^g, \sigma_m^g, f_m^g\right\}, \end{aligned} \tag{23}$$

and one is the 'old' parent as given in Eq.(20).

(III) **Selection**. In the final step, the CDF of the parent, CDF_P, and those of the offsprings, CDF_{O_l}, with $l = 1, 2, 3$, are generated. The set of parameters that fits the data best is the one whose CDFs minimizes the error given in Eq. (17). This set (either the old parent or one of the offsprings) is then selected to become the parent of the new generation X_P^{g+1} :

$$X_P^{g+1} = \left\{\mu_P^{g+1}, \sigma_P^{g+1}, f_P^{g+1}\right\} \tag{24}$$

$$X_P^{g+1} = \begin{cases} X_{O_l}^g & \text{if } Error(X_{O_l}^g) < Error(X_P^g), l = 1, 2, 3 \\ X_P^g & \text{otherwise} \end{cases} \tag{25}$$

Steps 1 to 3 are repeated until a prescribed tolerance is reached. In the current case, the set value was $\leq| \ 9 \cdot 10^{-5} \ |$. Thus, if the first four decimals of the parameters did not change in the last eight cycles, the most suitable distribution parameters were found. For every 10^y iterations, y being the number of fitted parameters, the scattering factor $\sigma(\alpha)$ is increased, if the number of successful offspring selections is higher than a set threshold (in this case, 0.2 out of the 10^y iterations [47]), otherwise the factor is decreased.

References

[1] Lewandrowski KU, Gresser JD, Wise DL, Trantol DJ. Bioresorbable bone graft substitutes of different osteoconductivities: a histologic evaluation of osteointegration of poly(propylene glycol-co-fumaric acid)-based cement implants in rats. Biomaterials 2000;21(8):757–64.

[2] Calori GM, Mazza E, Colombo M, Ripamonti C. The use of bone-graft substitutes in large bone defects: any specific needs? Injury 2011;42 Suppl 2:S56–63.

[3] Goulet JA, Senunas LE, DeSilva GL, Greenfield ML. Autogenous iliac crest bone graft. complications and functional assessment. Clin Orthop Relat Res 1997;339(339):76–81.

[4] Moore WR, Graves SE, Bain GI. Synthetic bone graft substitutes. ANZ J Surg 2001;71(6):354–61.

[5] Langer R, Vacanti J. Tissue engineering. Science 1993;260(5110):920–6.

[6] Hollister SJ. Porous scaffold design for tissue engineering. Nat Mater 2005;4(7):518–24.

[7] Hutmacher DW. Scaffolds in tissue engineering bone and cartilage. Biomaterials 2000;21(24):2529 –43. Orthopaedic Polymeric Biomaterials: Applications of Biodegradables.

[8] Griffith LG, Naughton G. Tissue engineering–current challenges and expanding opportunities. Science 2002;295(5557):1009–14.

[9] Roohani-Esfahani SI, Dunstan CR, Davies B, Pearce S, Williams R, Zreiqat H. Repairing a critical-sized bone defect with highly porous modified and unmodified baghdadite scaffolds. Acta Biomater 2012;8(11):4162–72.

[10] Fritsch A, Dormieux L, Hellmich C. Porous polycrystals built up by uniformly and axisymmetrically oriented needles: homogenization of elastic properties. Comptes Rendus Mecanique 2006;334(3):151 –7.

[11] Fritsch A, Dormieux L, Hellmich C, Sanahuja J. Mechanical behavior of hydroxyapatite biomaterials: An experimentally validated micromechanical model for elasticity and strength. Journal of Biomedical Materials Research Part A 2009;88A(1):149–61.

[12] Fritsch A, Hellmich C, Young P. Micromechanics-derived scaling relations for poroelasticity and strength of brittle porous polycrystals. Journal of Applied Mechanics 2013;80(2):020905–.

[13] Al-Hermezi HM, McKie D, Hall AJ. Baghdadite, a new calcium zirconium silicate mineral from iraq. Mineralogical Magazine 1986;50:119–23.

[14] Kohlhauser C, Hellmich C, Vitale-Brovarone C, Boccaccini AR, Rota A, Eberhardsteiner J. Ultrasonic characterisation of porous biomaterials across different frequencies. Strain 2009;45(1):34–44.

[15] Kohlhauser C, Hellmich C. Ultrasonic contact pulse transmission for elastic wave velocity and stiffness determination: Influence of specimen geometry and porosity. Engineering Structures 2013;47(0):115 –33. Special Issue in honour of Herbert Mang's 70th birthday: Selected papers from the Third International Symposium on Computational Mechanics in conjunction with the Second Symposium on Computational Structural Engineering (ISCM {III} - {CSE} II).

[16] Carcione JM. Wave fields in real media : wave propagation in anisotropic, anelastic, and porous media. First ed.; Oxford: Elsevier; 2001.

[17] Zaoui A. Continuum micromechanics: Survey. Journal of Engineering Mechanics 2002;128(8):808816.

[18] Dormieux L, Kondo D, Ulm FJ. Microporomechanics. Chichester: Wiley; 2006.

[19] De With G, Van Dijk H, Hattu N, Prijs K. Preparation, microstructure and mechanical properties of dense polycrystalline hydroxy apatite. Journal of Materials Science 1981;16(6):1592–8.

[20] Gilmore R, Katz J. Elastic properties of apatites. Journal of Materials Science 1982;17(4):1131–41.

[21] Liu DM. Preparation and characterisation of porous hydroxyapatite bioceramic via a slip-casting route. Ceramics International 1998;24(6):441 –6.

[22] Charriére E, Terrazzoni S, Pittet C, Mordasini P, Dutoit M, Lemaître J, et al. Mechanical characterization of brushite and hydroxyapatite cements. Biomaterials 2001;22(21):2937 –45.

[23] Malasoma A, Fritsch A, Kohlhauser C, Brynk T, Vitale-Brovarone C, Pakiela Z, et al. Micromechanics of bioresorbable porous cel2 glass ceramic scaffolds for bone tissue engineering. Advances in Applied Ceramics 2008;107(5):277–86.

[24] Ali M, Singh B. The effect of porosity on the properties of glass fibre-reinforced gypsum plaster. Journal of Materials Science 1975;10(11):1920–8.

[25] Phani K. Young's modulus-porosity relation in gypsum systems. American Ceramic Society Bulletin 1986;65:1584–6.

[26] Tazawa Ei. Effect of self stress on flexural strength of gypsum-polymer composites. Advanced Cement Based Materials 1998;7(1):1 – 7.

[27] Meille S. Étude du comportement mécanique du plâtre pris en relation avec sa microstructure. Ph.d. thesis; INSA de Lyon; 2001.

[28] Çolak A. Physical and mechanical properties of polymer-plaster composites. Materials Letters 2006;60(16):1977 –82.

[29] Craciun F, Galassi C, Roncari E, Filippi A, Guidarelli G. Electro-elastic properties of porous piezoelectric ceramics obtained by tape casting. Ferroelectrics 1998;205(1):49–67.

[30] Coble RL, Kingery WD. Effect of porosity on physical properties of sintered alumina. Journal of the American Ceramic Society 1956;39(11):377–85.

[31] Pabst W, Gregorová E, Tichá G, Týnová E. Effective elastic properties of alumina-zirconia composite ceramics-part 4. tensile modulus of porous alumina and zirconia. Ceramics-Silikáty 2004;48(4):165–74.

[32] Pabst W, Gregorová E, Tichá G. Elasticity of porous ceramics - a critical study of modulus-porosity relations. Journal of the European Ceramic Society 2006;26(7):1085 –97.

[33] Reynaud C, Thévenot F, Chartier T, Besson JL. Mechanical properties and mechanical behaviour of sic dense-porous laminates. Journal of the European Ceramic Society 2005;25(5):589 –97.

[34] Díaz A, Hampshire S. Characterisation of porous silicon nitride materials produced with starch. Journal of the European Ceramic Society 2004;24:413–9.

[35] Haglung J, Hunter OJ. Elastic properties of polycrystalline monoclinic Gd_2O_3. Journal of the American Ceramic Society 1973;56:327–30.

[36] Hum J, Luczynski KW, Nooeaid P, Newby P, Lahayne O, Hellmich C, et al. Stiffness improvement of 45S5 bioglass®-based scaffolds through natural and synthetic biopolymer coatings: An ultrasonic study. Strain 2013;49(5):431–9.

[37] Oliver W, Pharr G. An improved technique for determining hardness and elastic modulus using load and displacement sensing indentation experiments. Journal of Materials Research 1992;7:1564–83.

[38] Indentation Software User's Manual. CSM Instruments; Rue de la Gare 4 CH-2034 Peseux (Switzerland); 2008.
[39] Constantinides G, Chandran KR, Ulm FJ, Vliet KV. Grid indentation analysis of composite microstructure and mechanics: Principles and validation. Materials Science and Engineering: A 2006;430:189 – 202.
[40] Constantinides G, Ulm F. The nanogranular nature of c–s–h. Journal of the Mechanics and Physics of Solids 2007;55(1):64–90.
[41] Ulm FJ, Vandamme M, Bobko C, Alberto Ortega J, Tai K, Ortiz C. Statistical indentation techniques for hydrated nanocomposites: Concrete, bone, and shale. Journal of the American Ceramic Society 2007;90(9):2677–92.
[42] Malandrino A, Fritsch A, Lahayne O, Kropik K, Redl H, Noailly J, et al. Anisotropic tissue elasticity in human lumbar vertebra, by means of a coupled ultrasound-micromechanics approach. Materials Letters 2012;78(0):154 –8. 30th Anniversary Special Issue.
[43] Luczynski KW, Brynk T, Ostrowska B, Swieszkowski W, Reihsner R, Hellmich C. Consistent quasistatic and acoustic elasticity determination of poly-l-lactide-based rapid-prototyped tissue engineering scaffolds. Journal of Biomedical Materials Research Part A 2013;101A(1):138–44.
[44] Nix WD, Gao H. Indentation size effects in crystalline materials: A law for strain gradient plasticity. Journal of the Mechanics and Physics of Solids 1998;46(3):411 –25.
[45] Müllner HW, Fritsch A, Kohlhauser C, Reihsner R, Hellmich C, Godlinski D, et al. Acoustical and poromechanical characterisation of titanium scaffolds for biomedical applications. Strain 2008;44(2):153–63.
[46] Jaindl M, Reinbacher-Köstinger A, Magele C, Renhart W. Multi-objective optimization using evolution strategies. Series electronics and energetics 2009;22(2):159–74.
[47] Weicker K. Evolutionäre Algorithmen. Leitfäden der Informatik; Vieweg+Teubner Verlag; 2007. ISBN 9783835102194.

3 Future Outlook

The presented baghdadite scaffolds showed good mechanical properties, however, their brittleness is a concern.
Since this issue was already known to the producers of the scaffolds (Roohani-Esfahani et al., 2012), they also fabricated baghdadite scaffolds with a surface coating of polycaprolactone (PCL)/bioactive glass nanoparticles(nBGs). Scanning electron microscope images of the modified scaffolds revealed a smooth surface with the absence of cracks or pores.
The histological evaluation of a critical sized bone defect in a rabbit's ulna showed even better results than with uncoated baghdadite, the defect was better bridged and the volume of newly formed bone was higher. Future work could include the investigation of the mechanical properties of the coated scaffolds. The surface coating is expected to not only solve the brittleness issue, but also to enhance the mechanical properties of the baghdadite scaffolds.
The vast majority of approaches to develop new biomaterials are still based

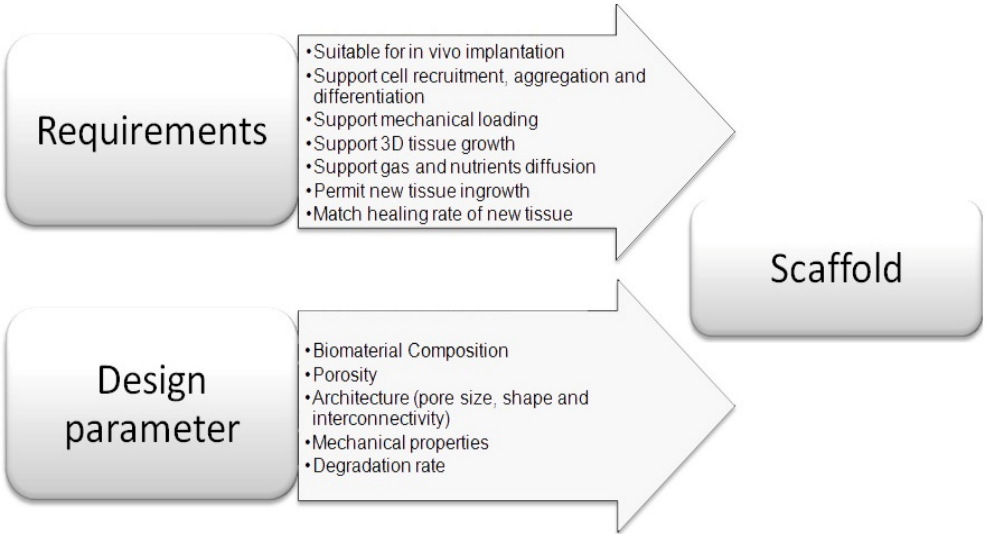

Figure 1: Essential input for scaffold design: requirements and parameters (adapted from Giannitelli et al. (2014))

on empirical trial and error (Lacroix et al., 2009), which has not changed since the beginning of the research field biomaterials. This tedious method is time-consuming and economically wasteful.

Consequently, more efficient and rational practices are necessary to succeed in designing better biomaterials for clinical use. Several factors play a key role in scaffold design (Fig.1), one of them being the mechanical properties of the material. The presented micromechanical model for brittle porous polycrystals (Fritsch et al., 2013) was able to predict the elastic modulus and Poisson's ratio reliably. The model can be used on its own or become an integrated part of a bigger application.

The current methods for computer-aided design and finite-element modelling of scaffolds for bone tissue engineering (Lacroix et al., 2009; Giannitelli et al., 2014) try to satisfy as many requirements as possible (see Fig.1).

Although the scaffold's requirements are conflicting, such as the need for high porosity for increased mass transport while also fulfilling high stiffness for mechanical support, an optimal trade-off needs to be found.

So far, there is no consensus on the ranges of optimal values for porosity, pore shape, dimension, and interconnectivity (Karande et al., 2004), there are only suggestions for minima values for porosity and pore size depending on the biomaterial and the defect location (Karageorgiou and Kaplan, 2005). Further research is necessary for understanding all the specifications in scaffold design.

Appendix A Sample Characterization

Table 1: Measurement, density, and porosity of baghdadite scaffolds

Sample	Weight [g]	Length[cm]	Diameter[cm]	Volume[cm^3]	ρ[g/cm^3]	Porosity[%]
A1	0.11	1.27	0.66	0.43	0.25	93
A2	0.08	1.24	0.60	0.35	0.22	94
A3	0.13	1.20	0.63	0.37	0.34	90
A4	0.11	1.26	0.61	0.37	0.29	92
A5	0.11	1.29	0.63	0.40	0.28	92
A6	0.10	1.17	0.67	0.41	0.25	93
A7	0.13	1.27	0.62	0.38	0.35	90
A8	0.08	1.19	0.61	0.34	0.22	94
B1	0.14	1.30	0.60	0.37	0.38	89
B2	0.15	1.27	0.65	0.42	0.36	90
B3	0.15	1.26	0.64	0.40	0.37	89
B4	0.14	1.35	0.62	0.41	0.35	90
B5	0.20	1.37	0.62	0.41	0.48	86
B6	0.13	1.20	0.63	0.37	0.36	90
B7	0.15	1.27	0.63	0.40	0.37	89
B8	0.21	1.34	0.63	0.42	0.51	85
B9	0.13	1.25	0.64	0.40	0.33	90
B10	0.20	1.35	0.65	0.45	0.44	87
B11	0.13	1.21	0.63	0.38	0.33	91
C1	0.24	1.27	0.63	0.39	0.61	82
C2	0.24	1.33	0.61	0.38	0.63	82
C3	0.27	1.21	0.66	0.41	0.67	81
C4	0.24	1.32	0.64	0.43	0.55	84
C5	0.27	1.27	0.68	0.46	0.59	83
C6	0.28	1.29	0.62	0.39	0.73	79
C7	0.22	1.16	0.62	0.35	0.62	82
C8	0.27	1.30	0.66	0.45	0.59	83
C9	0.22	1.30	0.64	0.41	0.53	85
C10	0.22	1.28	0.65	0.42	0.53	85
D1	0.52	1.35	0.66	0.46	1.14	67
D2	0.48	1.25	0.66	0.42	1.14	67
D3	0.46	1.25	0.64	0.40	1.13	67
D4	0.51	1.33	0.66	0.46	1.11	68
D5	0.45	1.25	0.65	0.41	1.10	68
D6	0.43	1.17	0.68	0.42	1.02	71
D7	0.42	1.21	0.68	0.43	0.97	72
D8	0.50	1.24	0.66	0.42	1.19	66

Appendix B Ultrasound test results

Table 2: Normal Stiffness C_{1111} of baghdadite scaffolds

Sample #	Porosity[%]	C_{1111}[GPa]
A1	93	1.17
A2	94	0.43
A3	90	1.03
A4	92	1.03
A5	92	1.15
A6	93	0.84
A7	90	1.61
A8	94	0.56
B1	89	1.55
B2	90	1.86
B3	89	1.79
B4	90	2.21
B5	86	2.84
B6	90	1.56
B7	89	1.96
B8	85	2.67
B9	90	1.75
B10	87	2.62
B11	91	1.12
C1	82	4.36
C2	82	4.76
C3	81	6.02
C4	84	3.03
C5	83	3.87
C6	79	5.09
C7	82	3.18
C8	83	3.20
C9	85	2.82
C10	85	3.39
D1	67	15.13
D2	67	16.57
D3	67	15.53
D4	68	15.65
D5	68	16.04
D6	71	10.48
D7	72	14.61
D8	66	17.27

Appendix C Mathlab code

C.1 Ultrasound data evaluation

```
% Experimental Data Bioceramic Baghdadite - Ca3ZrSi2O9
% Measurements & Weight & Acoustic Testing with
% Longitudinal waves 0.1 MHz
% 4 different Sets of Samples A-D with different porosities

% Sample Sets
A=[1 2 3 4 5 6 7 8];
B=[1 2 3 4 5 6 7 8 9 10 11];
C=[1 2 3 4 5 6 7 8 9 10];
D=[1 2 3 4 5 6 7 8];

% porosities for each Sample
por_A=[0.93 0.94 0.90 0.92 0.92 0.93 0.90 0.94];
por_B=[0.89 0.90 0.89 0.90 0.86 0.90 0.89 0.85 0.90 0.87 0.91];
por_C=[0.82 0.82 0.81 0.84 0.83 0.79 0.82 0.83 0.85 0.85];
por_D=[0.67 0.67 0.67 0.68 0.68 0.71 0.72 0.66];

% C1111 [GPa] for each Sample; Calculated through acoustic tests
% see Bioceramic_Ultrasound.xlsx
C11_A=[1.17 0.43 1.03 1.03 1.15 0.84 1.61 0.56];
C11_B=[1.55 1.86 1.79 2.21 2.84 1.56 1.96 2.67 1.75 2.62 1.12];
C11_C=[4.36 4.76 6.02 3.03 3.87 5.09 3.18 3.20 2.82 3.39];
C11_D=[15.13 16.57 15.53 15.65 16.04 10.48 14.61 17.27];

%create plot for C1111 obtained by ultrasound testing
%C1111.xls contains porosity (first column) &
%C1111 (second column)

num=xlsread('C1111');
% results devided into the four different sample sets
A=num(1:8,:);
B=num(9:19,:);
C=num(20:29,:);
D=num(30:end,:);


plot(A(1:end,1),A(1:end,2),'.',B(1:end,1),B(1:end,2),'+',
C(1:end,1),C(1:end,2),'*',D(1:end,1),D(1:end,2),'o');
axis([0.65 0.95 0.3 18]);
```

```
xlabel('Porosity $\phi$','fontname','arial','fontweight',
'normal','interpreter','latex','fontsize',14);
ylabel('$C_{1111}$ \rm{[GPa]}','fontname','arial','fontweight',
'normal','interpreter','latex','fontsize',14);
legend('A','B','C','D');

function [ myfit,gof ] = power_law()
%power law fit for data

C11=[1.17 0.43 1.03 1.03 1.15 0.84 1.61 0.56 ...
1.55 1.86 1.79 2.21 2.84...
1.56 1.96 2.67 1.75 2.62 1.12 4.36 4.76 6.02 ...
3.03 3.87 5.09 3.18 3.20...
2.82 3.39 15.13 16.57 15.53 15.65 16.04 ...
10.48 14.61 17.27];

por=[0.93 0.94 0.90 0.92 0.92 0.93 0.90 ...
0.94 0.89 0.90 0.89 0.90 0.86...
0.90 0.89 0.85 0.90 0.87 0.91 0.82...
0.82 0.81 0.84 0.83 0.79 0.82 0.83...
0.85 0.85 0.67 0.67 0.67 0.68 0.68 0.71 0.72 0.66];

roh=0:0.01:1;
x=por;
y=C11;

f=fittype('k*(1-x)^ce','coefficients',{'k','ce'},
'independent','x',...
'dependent','y');
coeffs = coeffnames(f);


options = fitoptions(f);
options.StartPoint = [0.5 1];
%options.Lower = [200 3];

[myfit,gof] = fit(x',y',f, options);
k=coeffvalues(myfit);


%calculation of c1111 for all porosites
%with calculated coefficients
C1111_expModel=k(1).*(1-roh).^ k(2);
```

```
hold on

axis=([0 0.95 0 18]);
xlabel=('\roh');
ylabel=('C11');

plot(roh,C1111_expModel,'k');
plot(myfit,'k',x,y)


end
```

C.2 Micromechanical model

```
function [es,ehom] = ehom()
%calculation of homogenized Young's modulus ehom
%for disc-type morphology
%inclusions depending on Young's modulus of single crystal es
por=0:0.01:1;
be=0.9867; %value from fritsch 2013
ce=2.053;   %value from frisch 2013
es=[75:1:152]; %range was chosen through literature research
ehom=zeros(length(es),length(por));

for i=1:1:length(es)
    ehom(i,:) =be*(1-por).^ce*es(i);
end
end

function [nus,nuhom] = nuhom()
%Calculation of homogenized poisson-ratio nuhom for
%disc-type solid inclusion
%based on given poisson-ratio nus of single crystal
%Calculation of nuhom depending on nus=0.25-0.29

por=0:0.01:1;
x=[-1.0521 2.2684 -0.8121 0.3602 0.2394];
y=[0.2197 -0.4645 0.1662 -0.0718 0.1496];
nus=[0.25:0.01:0.3];
nuhom=zeros(length(nus),length(por));

for i=1:1:length(nus);

    A=x(1)*nus(i)+y(1);
```

```
    B=x(2)*nus(i)+y(2);
    C=x(3)*nus(i)+y(3);
    D=x(4)*nus(i)+y(4);
    E=x(5)*nus(i)+y(5);

    nuhom(i,:)=A*(1-por).^4 + B*(1-por).^3 +
     C*(1-por).^2 + D*(1-por)+E;
end

end

function [ c1111 ] = func_c1111()
%calculating C1111
%using ehom & nuhom

[es,E]=ehom;
[nus,nu]=nuhom();
por=0:0.01:1;


%calculating c1111 for every possible combination of nu & E value

for i=1:1:size(nu,1)    %number of rows in nu
    for j=1:1:length(por)
        for k=1:1:size(E,1)%number of rows in E
            c1111(i,j,k)=(E(k,j).*(1-nu(i,j))) ./
            (((1+nu(i,j)).*(1-(2*nu(i,j)))));
        end
    end
end

end

function [] = err()
% error Calculation for calculated data c1111 and
% experimental data Cexp
% minimizing error to find most suitable Es and ns

clear;
clc;

Cexp=[1.17 0.43 1.03 1.03 1.15 0.84...
1.61 0.56 1.55 1.86 1.79 2.21 2.84...
1.56 1.96 2.67 1.75 2.62 1.12 4.36...
4.76 6.02 3.03 3.87 5.09 3.18 3.20...
```

```
2.82 3.39 15.13 16.57 15.53 15.65...
16.04 10.48 14.61 17.27];

por=[0.93 0.94 0.90 0.92 0.92 0.93...
0.90 0.94 0.89 0.90 0.89 0.90 0.86...
0.90 0.89 0.85 0.90 0.87 0.91 0.82...
0.82 0.81 0.84 0.83 0.79 0.82 0.83...
0.85 0.85 0.67 0.67 0.67 0.68 0.68...
0.71 0.72 0.66];

pos=por.*100;
cmodel=func_c1111();
cm=cmodel(:,pos(),:);
n=length(Cexp);
[e,eh] = ehom();
es=e(1,1);
[ns,nh]=nuhom();
nus=ns(1,1);
roh=0:0.01:1; %porosity



%mean absolute error mae
for i=1:1:size(cm,1)
    for k=1:1:size(cm,3)
        mae(i,k)= abs(sum(cm(i,:,k)-Cexp));
    end
end

[value_mae,location_mae] = min(mae(:));
%value&location of minimal mae
[R_mae,C_mae] = ind2sub(size(mae),location_mae);
es_mae=C_mae+es-1;
%value Young's modulus of single crystal es
nus_mae=(R_mae/100-0.01)+nus;
%value poisson-ratio of single crystal nus
min_mae=value_mae;

%mean error me
for i=1:1:size(cm,1)
    for k=1:1:size(cm,3)
        me(i,k)=sum(cm(i,:,k)-Cexp);
    end
end
```

```
[value_me,location_me] = min(me(:));
%value&location of minimal me
[R_me,C_me] = ind2sub(size(me),location_me);
es_me=C_me+es-1;
%value Young's modulus of single crystal es
nus_me=(R_me/100-0.01)+nus;
%value poisson-ratio of single crystal nus
min_me=value_me;


%sum of squared residuals s
for i=1:1:size(cm,1)
    for k=1:1:size(cm,3)
        s(i,k)=sum((cm(i,:,k)-Cexp).^2);
    end
end

[value_s,location_s] = min(s(:));
%value&location of minimal s
[R_s,C_s] = ind2sub(size(s),location_s);
es_s=C_s+es-1;
%value Young's modulus of single crystal es
nus_s=(R_s/100-0.01)+nus;
min_s=value_s;


%coefficient of determination of
%minimum mean absolute error mae
result_c=cm(R_mae,:,C_mae);
mean_Cexp=sum(Cexp)/length(Cexp);
sst_mae=sum((Cexp-mean_Cexp).^2);
ssr_mae=sum((Cexp-result_c).^2);
r2_mae=1-(ssr_mae/sst_mae);

%mean relative error
rerr_mae=(sum(1-(result_c./Cexp))/length(Cexp))*100;


%writing errors & Es and ns values into txt-file
err_cell={'Errortype' 'Error' 'E_{s}' '\nu_{s}';
            'mae',min_mae,es_mae,nus_mae;
            'me',min_me,es_me,nus_me;
            'ssr',min_s,es_s,nus_s;
            'R^2',r2_mae,es_mae,nus_mae ;
            'mean rel. error %',
```

```
            rerr_mae,es_mae,nus_mae};
fileID = fopen('error.txt','wt');
fprintf(fileID,'%s\t %s\t %s\t %s\n',err_cell{1,:});
for i=2:1:size(err_cell,1)
    fprintf(fileID,'%s\t %f\t %d\t %f\t\n',err_cell{i,:});
end
fclose(fileID);


%plotting
figure
z=s';
surf(ns,e,z);
xlabel('\nu_{s}');
ylabel('E_{s}');
zlabel('SSR');
colorbar;

figure
z2=mae';
surf(ns,e,z2);
xlabel('\nu_{s}');
ylabel('E_{s}');
zlabel('Mean Absolute Error');
colorbar


cplot_s=cmodel(R_s,:,C_s);
cplot_mae=cmodel(R_mae,:,C_mae);
figure
plot(roh,cplot_mae,por,Cexp,'ro');
xlabel('Porosity $\phi$','fontname',
'arial','fontweight',
'normal','interpreter','latex','fontsize',14);
ylabel('$C^{hom}_{1111}$ \rm{[GPa]}','fontname',
'arial','fontweight',
'normal','interpreter','latex','fontsize',14);
%L{1} = ['SSR: E_{s}= ' num2str(es_s) ' GPa
\nu_{s}= ' num2str(nus_s)];
L{2} = ['E^{model}_{s}= ' num2str(es_mae) ' GPa
\nu^{model}_{s}=
' num2str(nus_mae)];
L{3} =['Experimental Data'];

legend(L{2:3});
```

C.3 Nanoindendation data evalution

```
% plot nanoindentation data to receive
% load-displacement curve for a
% damaged crystal
% data from sample:A2_S1

n=xlsread('A2_S1_messung1.xls');
%time
t=n(:,1);
%displacement
d=n(:,2);
%force
f=n(:,3);

plot(d,f);
xlabel('Displacement [nm]','fontname','arial','fontweight',
'normal','interpreter','latex','fontsize',14);
ylabel('Load [GPa]','fontname','arial','font% plot
nanoindentation data to receive load-displacement curve for an
% intact crystal
% data from sample:D1_S3

num=xlsread('D1_S3_messung3');
%time
t=num(:,1);
%displacement
d=num(:,2);
%force
f=num(:,3);

plot(d,f);
xlabel('Displacement [nm]','fontsize',13);
ylabel('Load [GPa]','fontsize',13);weight',
'normal','interpreter','latex','fontsize',14);

% plot nanoindentation data to receive
% load-displacement curve for a
% damaged crystal
% data from sample:D1_S3

n=xlsread('D1_S3_messung4.xls');
%time
```

```
t=n(:,1);
%displacement
d=n(:,2);
%force
f=n(:,3);

plot(d,f);
xlabel('Displacement [nm]','fontname','arial','fontweight',
'normal','interpreter','latex','fontsize',14);
ylabel('Load [GPa]','fontname','arial','fontweight',
'normal','interpreter','latex','fontsize',14);

% plot nanoindentation data to receive
% load-displacement curve for an
% intact crystal
% data from sample:D1_S2, indentation #86,
% 10mN maximum load

num=xlsread('D1_S2_messung86');
%time
t=num(:,1);
%displacement
d=num(:,2);
%force
f=num(:,3);

plot(d,f);
xlabel('Displacement [nm]','fontname','arial','fontweight',
'normal','interpreter','latex','fontsize',14);
ylabel('Load [GPa]','fontname','arial','fontweight',
'normal','interpreter','latex','fontsize',14);


unction [hardness,emodulus,depth]=ReadFile(filename)
%reading data from txt-file constructed by csm nanoindenter


fileID=filename;
inputfile=fopen(fileID);

H='HIT='; %hardness
E='EIT='; %e-modulus
h='hmax='; %max. indentation depth
```

```
a=1;
b=1;
c=1;
tline = fgets(inputfile);


while tline~=-1

    if strfind(tline,H)
        %fprintf('%s', tline);
        hardness(a)=sscanf(tline,'%*s %f %*s');
        a=a+1;
    end
    if strfind(tline,E)
        %fprintf('%s', tline);
        emodulus(b)=sscanf(tline,'%*s %f %*s');
        b=b+1;
    end
    if strfind(tline,h)
        %fprintf('%s', tline);
        depth(c)=sscanf(tline,'%*s %f %*s');
        c=c+1;
    end
    tline=fgets(inputfile);

end
fclose(inputfile);


function [p,steps,s] = test_evolution()
% written to test if evolution algorithm

data=normrnd(50,2,1,400);

xd=ecdf(data);
xd=(xd(2:end))';

z=normrnd(0,1,1,100);
s=[1.7 0.3];
h=0.3;

p=[40 1]; %parents
k=0; % counting variable
n=0; % counting variable
tol=0.00009; % tolerance
```

```
for i=1:length(z)
    o=p+ s*z(i); %offspring

    xp=normcdf(data,p(1),p(2));
    xo=normcdf(data,o(1),o(2));

    ep=sum((xp-xd).^2);
    eo=sum((xo-xd).^2);

    if  eo < ep
        p=o;
        k=k+1;
    end

    if (mod(i,10)==0)
        n=n+1;
        if (k*n < 4*n)
            s=s/h;
        end
        if (k*n > 4*n)
            s=s*h;
        end
    end

    err(i)=xp(1);

    if (i>99) && (err(i)-err(i-1) + err(i-2)-err(i-3) +
    err(i-4)-err(i-5) < tol);
        steps=i;
        break;
    end
end

end


function [error_p,p,w,r2,r] = cdf_five_distributions()
% nanoindentation data fitting of 15 parameters made up of
% 5 normal distributions with mean value and standard deviation
% every distribution has a weighting factor,
% (1,lambda)- evolution strategy


filename='emodulus_allSamples.mat';
```

```
e=load(filename);
e=sort(e.e);
e_u=unique(e);

[f,x_e]=ecdf(e);
f=f';
x_e=x_e';

% parent values for evolution
p=[14.50 7.50 44.50 15.50 65.00 22.00 89.00 18.50 128.00 33.50];
o=zeros(1,10); % offspring
% weighting factors, sum=1
w1=0.31;
w2=0.15;
w3=0.14;
w4=0.11;
w5=1-(w1+w2+w3+w4);
w=[w1 w2 w3 w4 w5];
wn=zeros(1,5);

z=zeros(10, 20000); % creating 10 distributions
% because 10 parameters need to be optimised
for i=1:10
    z(i,:)=normrnd(0,1,1,20000);
end

wz=zeros(5,20000);
% creating 5 distributions for 5 weighting factors
for i=1:5
    wz(i,:)=rand(1,20000);
end


s=[0.09 0.05 0.04 0.08 0.03 0.10 0.13 0.02 0.30 0.07];
% scattering for p
sw=[1.001 1.002 1.006 1.005 1.003];
% scattering for w
h=0.85; % stepsize

k=0; % counter
t=0;
tol=0.00009; %tolerance
pm=ones(1,8);

for i=1:size(z,2)
```

```
%creating offspring=mutation
for j=1:size(z,1)
o(j)=p(j)+(s(j)*z(j,i)); %mutation
end

%mutation of weighting factor
for j=1:size(wz,1)
   wn(j)=w(j)+(sw(j)*wz(j,i));
end

while (sum(wn)~=1) % sum of w must be 1!!
    wn=wn/sum(wn);
    t=t+1;
    if (t>1000)
       break;
    end
end

x_p1=normcdf(e_u,p(1),p(2));
x_p2=normcdf(e_u,p(3),p(4));
x_p3=normcdf(e_u,p(5),p(6));
x_p4=normcdf(e_u,p(7),p(8));
x_p5=normcdf(e_u,p(9),p(10));
x_p=(w(1).*x_p1)+(w(2).*x_p2)+(w(3).*x_p3)+
(w(4).*x_p4)+(w(5).*x_p5);

%calculating offspring with original distribution
%& mutated weighting
x_pn=(wn(1).*x_p1)+(wn(2).*x_p2)+(wn(3).*x_p3)+
(wn(4).*x_p4)+(wn(5).*x_p5);


%calculating offspring with mutated distribution
%& original weighting

x_o1=normcdf(e_u,o(1),o(2));
x_o2=normcdf(e_u,o(3),o(4));
x_o3=normcdf(e_u,o(5),o(6));
x_o4=normcdf(e_u,o(7),o(8));
x_o5=normcdf(e_u,o(9),o(10));
x_o=(w(1).*x_o1)+(w(2).*x_o2)+(w(3).*x_o3)+...
(w(4).*x_o4)+(w(5).*x_o5);

%calculating offspring with mutated distribution
```

```
& mutated weighting
x_on=(wn(1).*x_o1)+(wn(2).*x_o2)+(wn(3).*x_o3)+...
(wn(4).*x_o4)+(wn(5).*x_o5);



e_p=zeros(length(x_p));
e_pn=zeros(length(x_pn));
e_o=zeros(length(x_o));
e_on=zeros(length(x_on));

for j=1:length(x_p)
    e_p(j)=(x_p(j)-f(j+1))^2;
end
error_p=sum(e_p(:));

for j=1:length(x_pn)
    e_pn(j)=(x_pn(j)-f(j+1))^2;
end
error_pn=sum(e_pn(:));

 for j=1:length(x_o)
    e_o(j)=(x_o(j)-f(j+1))^2;
end
error_o=sum(e_o(:));

for j=1:length(x_on)
    e_on(j)=(x_on(j)-f(j+1))^2;
end
error_on=sum(e_on(:));

err=[error_p error_pn error_o error_on];
% find minimum error to decide
%parents for next generation
if (min(err)==err(2))
    w=wn;
end
if (min(err)==err(3))
    p=o;
    k=k+1;
end
if(min(err)==err(4))
    p=o;
    w=wn;
    k=k+1;
```

```
    end

    if (mod((i/14),10)==0)
    %14=number of independently fitted paramters

        if (k < 8) % 1/5 sucess rule
            s=s/h; % adopt step size
            sw=sw/h;
        end
        if (k > 8)
            s=s*h;
            sw=sw/h;
        end
    end

     if (mod((i/14),10)==0)
        k=0;   %reset counter
     end

     pm(i)=p(9);

     if (i>7) && (pm(i-7)-pm(i-6) + pm(i-5)-pm(i-4) +
      pm(i-3)-pm(i-2) + pm(i-1)-pm(i) < tol)
         break;
     end

end
%coefficient of determination
mean=sum(f)/length(f);
sst=sum((f-mean).^2);
ssr=sum((f(2:end)-x_p).^2);
r2=1-(ssr/sst);

%relative error in percent
r=sum(1-(x_p/f(2:end)))*100;

%plot
y_xp1=w1.*x_p1;
y_xp2=w2.*x_p2;
y_xp3=w3.*x_p3;
y_xp4=w4.*x_p4;
y_xp5=w5.*x_p5;
y_k=y_xp1+y_xp2+y_xp3+y_xp4+y_xp5;
```

```
figure
plot(e_u,y_xp1,e_u,y_xp2,e_u,y_xp3,
e_u,y_xp4,e_u,y_xp5,e_u,y_k);
hold on
plot(x_e,f);
hold off
end


% plotting histogram and fitted distributions
p=load('Distribution_Values');
p=p.p;
w=load('weightingFactors');
w=w.w;
e=load('emodulus_allSamples');
e=sort(e.e);

% probability density function
y1=normpdf(e,p(1),p(2));
y2=normpdf(e,p(3),p(4));
y3=normpdf(e,p(5),p(6));
y4=normpdf(e,p(7),p(8));
y5=normpdf(e,p(9),p(10));


y1=w(1)*y1;
y2=w(2)*y2;
y3=w(3)*y3;
y4=w(4)*y4;
y5=w(5)*y5;
y=y1+y2+y3+y4+y5;

d=6.7;
range=min(e):d:max(e);
[n,xe]=histc(e,range);
ye=n/(sum(n)*d);

ed=min(e):5:max(e);
yd=min(y):5:max(y);
figure
bar(range,ye,'histc'); %--> area=1
hold on
plot(e,y,'r-')
plot(e,y1,e,y2,e,y3,e,y4,e,y5)
%plot(ed,yd,'g.')
```

```
hold off

axis([0 max(e) 0 0.018]);
xlabel('Elastic modulus [GPa]','fontname',...
'arial','fontweight','normal','interpreter',
'latex','fontsize',24);
ylabel('Density','fontname',...
'arial','fontweight','normal','interpreter',
'latex','fontsize',24);


%plot cdf
e_u=unique(e);

[f,x_e]=ecdf(e);
f=f';
x_e=x_e';

x_p1=normcdf(e_u,p(1),p(2));
x_p2=normcdf(e_u,p(3),p(4));
x_p3=normcdf(e_u,p(5),p(6));
x_p4=normcdf(e_u,p(7),p(8));
x_p5=normcdf(e_u,p(9),p(10));

y_xp1=w(1).*x_p1;
y_xp2=w(2).*x_p2;
y_xp3=w(3).*x_p3;
y_xp4=w(4).*x_p4;
y_xp5=w(5).*x_p5;
y_k=y_xp1+y_xp2+y_xp3+y_xp4+y_xp5;


figure
plot(x_e,f,'r:',e_u,y_k,'b',e_u,y_xp1,'b',e_u,y_xp2,'b',...
e_u,y_xp3,'b',e_u,y_xp4,'b',e_u,y_xp5,'b');
grid on;
xlabel('Elastic modulus [GPa]','fontname','arial',...
'fontweight','normal','interpreter','latex','fontsize',24);
ylabel('CDF','fontname','arial','fontweight',...
'normal','interpreter','latex','fontsize',24);
legend('Experimental','Theoretical')
```

References

Calori, G. M., Mazza, E., Colombo, M., and Ripamonti, C. (2011). The use of bone-graft substitutes in large bone defects: any specific needs? *Injury*, 42 Suppl 2:S56–S63.

De Aza, P., Fernandez-Pradas, J., and Serra, P. (2004). In vitro bioactivity of laser ablation pseudowollastonite coating. *Biomaterials*, 25(11):1983–1990. cited By (since 1996)37.

Fritsch, A., Hellmich, C., and Young, P. (2013). Micromechanics-derived scaling relations for poroelasticity and strength of brittle porous polycrystals. *Journal of Applied Mechanics*, 80(2):020905–020905.

Giannitelli, S., Accoto, D., Trombetta, M., and Rainer, A. (2014). Current trends in the design of scaffolds for computer-aided tissue engineering. *Acta Biomaterialia*, 10(2):580 – 594.

Goulet, J. A., Senunas, L. E., DeSilva, G. L., and Greenfield, M. L. (1997). Autogenous iliac crest bone graft. complications and functional assessment. *Clin Orthop Relat Res*, 339(339):76–81.

Hench, L. L. and Thompson, I. (2010). Twenty-first century challenges for biomaterials. *Journal of The Royal Society Interface*, 7:379–391.

Jones, J. R. (2013). Review of bioactive glass: from hench to hybrids. *Acta Biomater*, 9(1):4457–4486.

Karageorgiou, V. and Kaplan, D. (2005). Porosity of 3d biomaterial scaffolds and osteogenesis. *Biomaterials*, 26(27):5474 – 5491.

Karande, T., Ong, J., and Agrawal, C. (2004). Diffusion in musculoskeletal tissue engineering scaffolds: Design issues related to porosity, permeability, architecture, and nutrient mixing. *Annals of Biomedical Engineering*, 32(12):1728–1743.

Kulakov, O., Doktorov, A., Diakova, S., Denisov-Nikolskiy, Y., and Gratz, K. (2005). Experimental study of osseointegration of zirconium and titanium dental implants. *Morfologiya*, 127:52–55.

Lacroix, D., Planell, J. A., and Prendergast, P. J. (2009). Computer-aided design and finite-element modelling of biomaterial scaffolds for bone tissue engineering. *Philosophical Transactions of the Royal Society A: Mathematical,Physical and Engineering Sciences*, 367(1895):1993–2009.

Levert, H. S. (1829). Experiments on the use of metallic ligatures, as applied to arteries. *The American Journal of the Medical Sciences*, 7:17–22.

Lewandrowski, K. U., Gresser, J. D., Wise, D. L., and Trantol, D. J. (2000). Bioresorbable bone graft substitutes of different osteoconductivities: a histologic evaluation of osteointegration of poly(propylene glycol-co-fumaric acid)-based cement implants in rats. *Biomaterials*, 21(8):757–764.

Moore, W. R., Graves, S. E., and Bain, G. I. (2001). Synthetic bone graft substitutes. *ANZ J Surg*, 71(6):354–361.

Ramaswamy, Y., Wu, C., Hummel, A. V., Combes, V., Grau, G., and Zreiqat, H. (2008). The responses of osteoblasts, osteoclasts and endothelial cells to zirconium modified calcium-silicate-based ceramic. *Biomaterials*, 29(33):4392 – 4402.

Ratner, B., Hoffman, A., Schoen, F., and Lemons, J. (2004). *Biomaterials Science: An Introduction to Materials in Medicine*. Elsevier Science.

Roohani-Esfahani, S. I., Dunstan, C. R., Davies, B., Pearce, S., Williams, R., and Zreiqat, H. (2012). Repairing a critical-sized bone defect with highly porous modified and unmodified baghdadite scaffolds. *Acta Biomater*, 8(11):4162–4172.

Vallet-Regi, M. (2006). Revisiting ceramics for medical applications. *Dalton Trans.*, pages 5211–5220.

Zierold, A. A. (1924). Reaction of bone to various metals. *Archives of Surgery*, 9(2):365–412.